

# $\omega$ -functionalized self-assembled monolayers chemisorbed on ultraflat Au(111) surfaces for biological scanning probe microscopy in aqueous buffers

Peter Wagner,<sup>a)</sup> Frank Zaugg, Peter Kernen, Martin Hegner,<sup>b)</sup> and Giorgio Semenza  
Department of Biochemistry, Swiss Federal Institute of Technology, ETH Zentrum,  
CH 8092 Zurich, Switzerland

(Received 25 July 1995; accepted 16 October 1995)

Two immobilization procedures for ultimately carrying out scanning probe microscopy of native biological macromolecules in buffer solution are presented. They are based on the preparation of ultraflat template-stripped gold surfaces and subsequent chemisorption of bioreactive  $\omega$ -functionalized self-assembled monolayers. Immobilization was achieved either via amide bond formation or diazo linkage. The first was carried out using a long-chain N-hydroxysuccinimide-ester functionalized disulfide, which binds amino-group-containing biomacromolecules under mild conditions. The latter was performed via chemisorption of a nitrobenzylalkylthiol, followed by *in situ* transformation to the active diazo intermediate. Typical targets were activated aromatic hydrogens, such as phenolic or imidazole groups. The preparation of these monolayers, their characterization by scanning tunneling microscopy and radiolabeling, and as an example the *in situ* atomic force microscopy study of clathrin cages under native conditions in appropriate buffers are presented. © 1996 American Vacuum Society.

## I. INTRODUCTION

Immobilization of biomolecules on solid surfaces has been widely used for affinity chromatography and solid-phase analytical techniques; however, applications such as biosensor devices, supramolecular systems, scanning probe microscopy (SPM), and nanostructure technologies require more sophisticated approaches with well-defined molecular architecture on a nm scale. Organic compounds which associate spontaneously to well-ordered molecular assemblies at the solid-liquid interface could be a valuable tool toward this goal. During the last decade self-assembled monolayers (SAMs) of alkanethiols and disulfides based on the strong coordination of sulfur on gold have been studied with an impressive pace.<sup>1-3</sup> The structures of these monolayers have been thoroughly investigated mainly by infrared spectroscopy,<sup>4,5</sup> diffraction techniques,<sup>6-11</sup> wetting measurements,<sup>2,3,12</sup> ellipsometry,<sup>13</sup> and SPM;<sup>14-23</sup> however, far fewer studies exist to date on functionalized SAMs. If  $\omega$  substituted, these monolayers would provide valuable tools for the construction of multilayer assemblies and the immobilization of biological structures.<sup>24-28</sup> Here we present two procedures for ultimately carrying out SPM of native biological macromolecules in buffer solution using a combination of

- (i) molecular self-assembly;
- (ii) preparation of ultraflat Au(111) surfaces; and
- (iii) chemical functionalization.

One approach is based on the *ex situ* synthesis of dithiobis(succinimidyl-undecanoate) DSU I providing a

long-chain N-hydroxysuccinimide-ester functionalized dialkyldisulfide SAM I, which is accessible for nucleophilic attack (e.g., amide bond formation with amino-group-containing molecules). A second route alternatively allows the immobilization of activated aromatic rings such as phenol (Tyr) and imidazole (His) via *in situ* diazonium chemistry using 11-mercapto-4-nitrobenzyl-undecanoate II as precursor SAM II. These two paths cover most requirements since several different amino-acid residues are appropriate targets. Furthermore, the strategy of using two highly reactive SAMs with different specificity would allow, if chemisorbed from mixtures, the selective and versatile immobilization of ligands and effectors in multistep procedures. Here we present the preparation of both SAMs, their characterization with scanning tunneling microscopy (STM) and radiolabeling, and as an example the *in situ* atomic force microscopy (AFM) imaging of the disassembly of clathrin cages under native conditions anchored on SAM I.

## II. EXPERIMENT

All solvents and chemicals were of highest purity. The preparation of ultraflat, polycrystalline Au(111) surfaces [template-stripped gold (TSG)] was carried out as previously described.<sup>28,29</sup> Immersion of TSG surfaces into a 1 mM solution of I and II in 1,4-dioxane (freshly distilled) at room temperature for 60 min provided the corresponding monolayers. After rinsing with 5-7 ml 1,4-dioxane, the monolayers were dried under a stream of nitrogen and immediately used for analyses, immobilization of amino acids, or further activation steps. The *in situ* synthesis of the diazo-derivative IV (see also Fig. 3) was performed in the reaction chamber (see Fig. 4) by first conversion of the nitrobenzyl compound II to the aminobenzyl intermediate III by treatment with a 10% (wt/vol) solution of sodium dithionite (15 h, 20 °C). Addition of cold (<5 °C, 30 min) acidic sodium nitrite (0.5 M NaNO<sub>2</sub>)

<sup>a)</sup> Author to whom correspondence should be addressed. Present address: Dept. Biochemistry, Beckman Ctr B 405, Stanford University School of Medicine, Stanford, CA 94305-5307.

<sup>b)</sup> Additional address: Institute of Physics, University of Basel, Klingelbergstrasse 82, CH-4056 Basel, Switzerland.

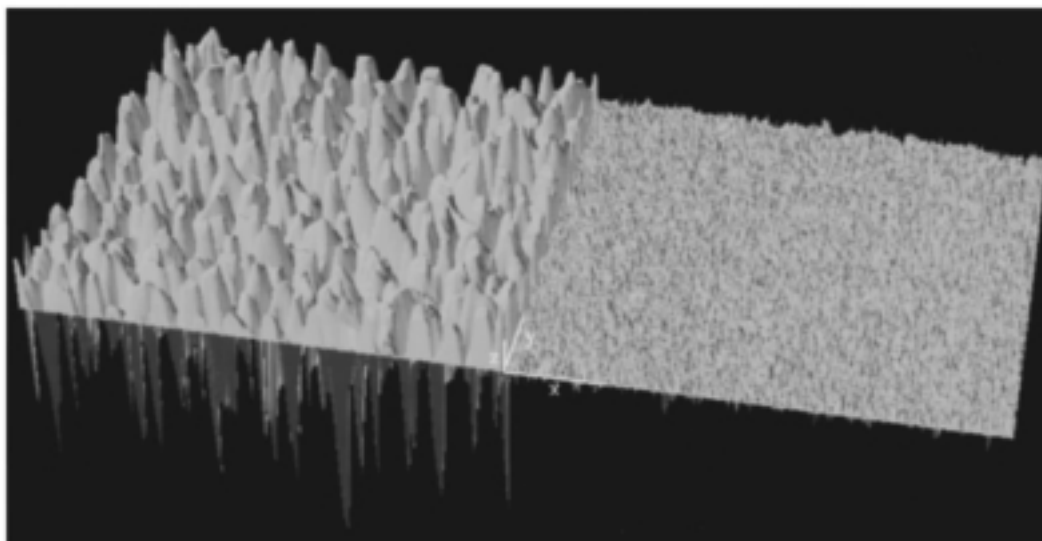


FIG. 1. STM images of gold surfaces (1 nA, 200 mV) prepared by thermal evaporation. Left-hand side: conventionally prepared gold surface, deposited at 250 °C on mica; right-hand side: typical ultraflat template-stripped gold surface, deposited at room temperature on mica;  $x=y=1\ \mu\text{m}$ ;  $z=2\ \text{nm}$ .

in 0.5 M HCl) resulted in the formation of the reactive diazo compound IV. Immobilization as a function of  $p\text{H}$  was determined with  $[\text{U-}^{14}\text{C}]\text{-L-lysine}$  on SAM I and with  $[\text{U-}^{14}\text{C}]\text{-L-tyrosine}$  and  $[\text{U-}^{14}\text{C}]\text{-L-histidine}$  on SAM IV. A drop of 50  $\mu\text{l}$  of a 1 mM solution of lysine (specific activity adjusted to 26.6 mCi/mmol), tyrosine (specific activity of 9.95 mCi/mmol), or histidine (specific activity of 12.04 mCi/mmol) in 50 mM phosphate buffer ( $p\text{H}$  ranging from 6.5 to 8.5) or 50 mM borate buffer ( $p\text{H}\geq 8.5$ ) was applied onto a 1  $\text{cm}^2$  sample of SAM I and SAM IV and placed into a chamber with 100% humidity. After 16 h the samples were thoroughly rinsed (10 times with 2 ml coupling buffer), air dried, and subjected to PhosphorImaging®. Quantification was carried out using air-dried standards of the corresponding amino acids. AFM was performed on a Nanoscope III from Digital Instruments, Inc. (Santa Barbara, CA). Microfabricated monocrystalline silicon tips were used with force constants ranging from 0.02 to 0.66 N/m (LOT, Darmstadt, Germany). STM was carried out on a Nanoscope III from Digital Instruments, Inc. (Santa Barbara, CA) with a modified STM tip-view head for a tunneling resistance limit of 0.1 T $\Omega$ . Mechanically cut PtIr tips (80/20) were used for imaging of ultraflat gold surfaces and monolayers. The *in situ* disassembly of clathrin cages was previously described.<sup>30</sup>

### III. RESULTS AND DISCUSSION

As substrates for the formation of  $\omega$ -functionalized monolayers we used ultraflat polycrystalline Au(111) surfaces (TSGs), which are particularly suitable for biological applications. The small roughness of these TSG surfaces (typically 0.2–0.5 nm per 100  $\mu\text{m}^2$ ) is based on the deposition of gold onto mica, followed by removal of the flat mica. The gold layer which is eventually used as substrate is the very first one having been deposited on the mica template. The procedure for the removal of the mica platelet (“stripping”) and the structural characterization of the resulting TSG sur-

faces have been reported in detail in previous publications.<sup>28,29</sup> The STM image of Fig. 1 shows a 3D comparison of a conventional gold surface (left-hand side) and a typical TSG surface (right-hand side). The main characteristic structural feature is the completely annealed surface, comprising terraces with diameters of 50–500 nm, differing only in 3–5 atomic steps in  $z$  height [see also Fig. 5(A)]. This lack of deep grooves and holes having extremely large differences in  $z$  heights as normally present on conventional gold substrates (Fig. 1, left-hand side) would provide a better packing of chemisorbed molecules and make SPM imaging of fibrillary structures on TSGs easier. Atomic resolution STM images proved the heteroepitaxial nature of these Au(111) films showing the hexagonal (111) orientation and lattice spacings of 0.288 and 0.499 nm for the nearest- and the next-nearest-neighbor distance, respectively (data not shown). X-ray photoelectron spectroscopy (XPS) analyses showed that only trace amounts of Si and Al from the original mica were left on the Au(111) surface (data not shown).

The use of  $\omega$ -functionalized monolayers on ultraflat gold surfaces provides highly reactive interfaces and enables the control of reactivity and hydrophobicity of these surfaces. Moreover, more sophisticated immobilization strategies should be possible, such as reversible anchoring, multiple reactivities, and site-specific immobilization. Figure 2 outlines the self-assembly of compound I to a tightly packed monolayer arrangement. This monolayer has proven its value in several SPM studies of native biomacromolecules (e.g., see Refs. 30 and 31) and was carefully characterized by SPM, radiometry, contact angle measurements, reflection infrared spectroscopy, and ellipsometry.<sup>32</sup> These studies showed that SAM I consists of a densely packed arrangement with a maximum binding site density of 585 pmol/ $\text{cm}^2$  (which represented 75% of the theoretical value of a hexagonally close-packed, nonfunctionalized alkanethiol), and a long duration reactivity (hours–days) toward nucleophilic

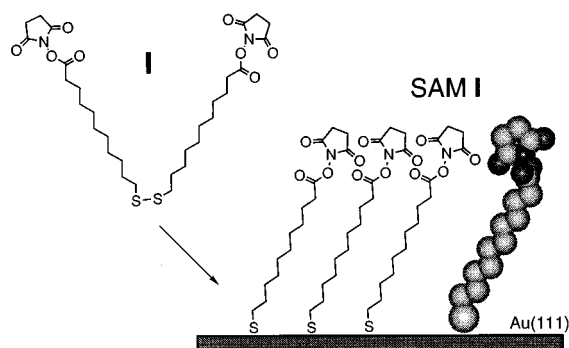


Fig. 2. Self-assembly of compound I (DSU) to a tightly packed monolayer on Au(111). The tilt angle of the hydrocarbon chains and the nature of the S—Au bonds are drawn fictitiously.

groups. The kinetics of monolayer formation is very fast (complete coverage within seconds), whereas the kinetics of reactivity is much slower than for N-hydroxysuccinimide esters in solution.

The second approach presented in this article is the diazo linkage between aromatic residues with activated hydrogens and the aryldiazonium electrophilic groups of SAM IV. Hence, the primary structural targets are phenolic (Tyr) and imidazole (His) groups, and of secondary importance the attack of guanidino groups (Arg) and indole (Trp). This monolayer was prepared as shown in Fig. 3. The starting compound 11-mercapto-4-nitrobenzyl-undecanoate II was chemisorbed via thiolate bonding on TSG surfaces providing a SAM of *p*-nitrobenzylalkyl groups. The active diazonium derivative SAM IV was accomplished through an *in situ* multistep transformation of SAM II, i.e., by first reduction of the nitroaryl group to the amino precursor SAM III using sodium dithionite and subsequent conversion to SAM IV by treatment with cold acidic nitrite solution. Coupling to the phenol- or imidazole-containing molecule (here tyrosine and histidine) was achieved under slightly basic conditions below 5 °C. If necessary, the resulting azo linkage could be reduced to liberate again the immobilized molecule (not shown in Fig. 3). All reaction steps were done in a special reaction chamber (Fig. 4) consisting of a glass tube of 8 mm inner diameter pressed via a Kalrez® O-ring onto the template-stripped gold surface. The upper part is widened to increase the reaction volume and can accommodate a Pt100 thermometer for temperature control, a heating/cooling system, and, on the top, a Teflon seal for the injection of reagents.

Figures 5(A)–5(D) show 500×500 nm<sup>2</sup> STM images of (A) a typical TSG surface and (B) SAMs I, (C) II, and (D) III taken in the constant-current mode at ambient conditions. The structural topographies of the SAMs reflect those of the underlying gold surfaces concerning shape and size of terraces. These are separated by monoatomic steps and exhibit the typical depressions, which are single-atom deep pits resulting from an etching process during the adsorption of the sulfur compound.<sup>14,20,33,34</sup> The apparently less frequent depressions in Fig. 5(B) of SAM I compared to SAM II do not represent a lower degree of etching by the disulfide I com-

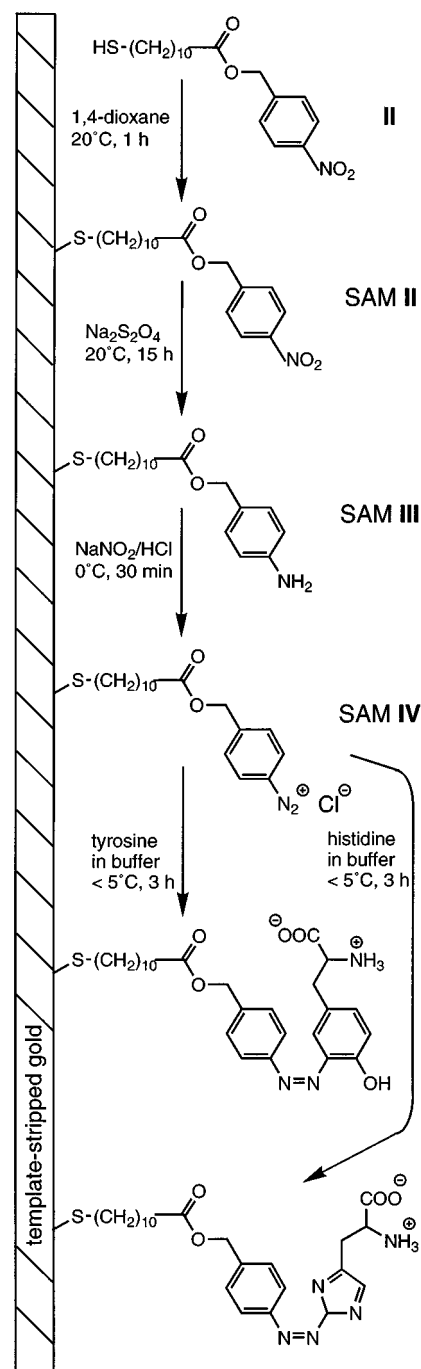


Fig. 3. Reaction scheme of the *in situ* synthesis of SAM IV, and coupling of the diazo derivative with tyrosine and histidine, respectively.

pared to thiol II. Also, the triangular facets in Fig. 5(D) of SAM III resulting from the (111) orientation are not exclusively characteristic for SAM III since they could also often be recognized in uncovered TSGs or on SAMs I and II. The lack of atomic-scale resolution of these monolayers makes it difficult to obtain detailed information from SPM alone on packing density, monolayer arrangement, and defect structures in contrast to SPM imaging of nonfunctionalized alkanethiol SAMs where the hexagonal ( $\sqrt{3}\times\sqrt{3}$ )R30° over-

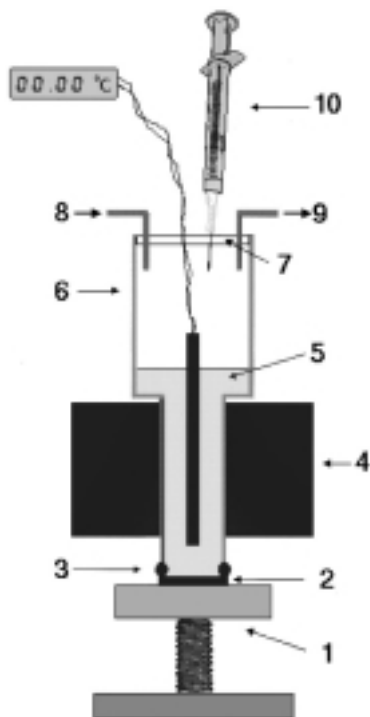


FIG. 4. Reaction chamber for *in situ* synthesis, analyses, and modification of SAMs on TSG. 1: PTFE base; 2: template-stripped gold film; 3: Kalrez® O-ring; 4: heating/cooling coat; 5: reaction medium with Pt100 thermosensor; 6: reaction chamber (glass); 7: silicone seal; 8: inert gas inlet; 9: inert gas outlet; 10: syringe for reagents. For *in situ* synthesis of SAM IV, items 7–10 have not been used.

layer structure with  $c(4 \times 2)$  superlattices, as well as domain structures, could be routinely achieved (if performed in the  $T\Omega$  range).<sup>14–23,28</sup> The absence of molecular resolution of SAMs I, II, and III is primarily caused by the polar and bulky groups in  $\omega$  position, which are often covered with coadsorbates, but is also due to imperfections and collapsed sites, as well as tip penetration (despite the increased tunneling resistance of our microscope). However, together with the ellipsometrical and wetting data (not shown) one can draw the conclusion that indeed compounds I and II formed monolayers, and *in situ* transformation ran to completion.

The reactivity of SAMs I and IV toward appropriate amino acids was monitored by reacting with <sup>14</sup>C-labeled lysine, tyrosine, and histidine with subsequent quantification by PhosphorImaging®. In previous studies we have thoroughly investigated the binding characteristics of SAM I.<sup>32</sup> This monolayer showed high capacity and reactivity, but slow kinetics of the reaction, which makes it easy to control the amount of immobilized biomolecules. Therefore, also very rare biomolecules can be successfully immobilized (protein concentrations as low as 10–1000 ng/ml). The *pH* dependence of [<sup>14</sup>C]–lysine binding on SAM I [see Fig. 6(A)] showed a tenfold increase in reactivity with increasing *pH* from 6.5 to 8.5 due to increased deprotonation of the amino groups and accelerated binding attributed to limited hydrolysis.<sup>32</sup> The amount of bound lysine was in the range of tens of pmol per cm<sup>2</sup>, which is approximately 5% of the

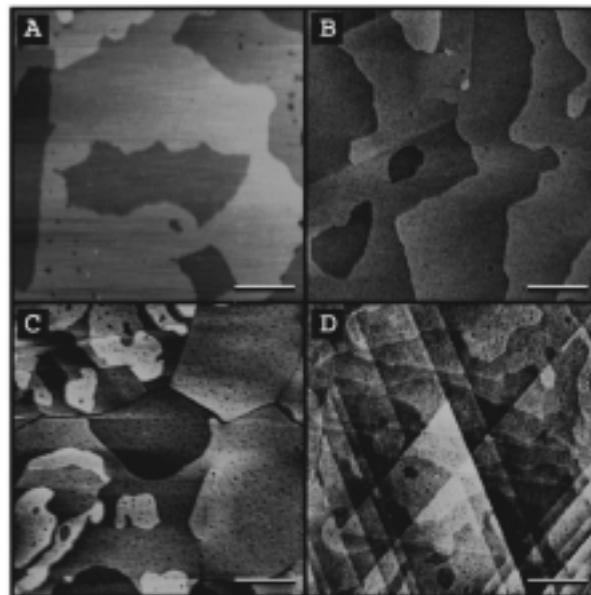


FIG. 5. STM images (9 pA, 1 V) of (A) a TSG surface and (B) SAMs I, (C) SAM II, and (D) SAM III; bars: 500 nm; *z* range: 3 nm.

binding sites theoretically available. Immobilization of [<sup>14</sup>C]–tyrosine on SAM IV showed a similar *pH* dependence, because of the increasing concentration of phenolate anions with increasing *pH*. In comparison, however, SAM IV bound ten times more amino acid (tyrosine) than did SAM I (lysine), i.e., up to more than 500 pmol/cm<sup>2</sup> at *pH* 10, which is nearly 100% coupling efficiency. This could be attributed to an increase of the accessibility for attacking the diazo group compared to the more hidden *sp*<sup>2</sup> carbons of SAM I and is subject of further investigations. The total amount of bound [<sup>14</sup>C]–histidine is much lower and shows no obvious *pH* dependence.

As an example for the applicability of SAM I we have carried out the first *in situ* AFM study of the disassembly of clathrin cages [Fig. 7(A)] under native conditions (see also Ref. 30). This protein forms the regular polyhedral surface lattice of clathrin-coated vesicles, which is involved in intracellular protein transport. The disintegration of the cages to the typical three-legged clathrin protomers (triskelia) [Fig. 7(C)] could be followed at the liquid–solid interface. The slower kinetics of the disassembly compared to the process in solution made it possible even to observe an intermediate basketlike structure [Fig. 7(B1)–7(B4)].

#### IV. CONCLUSION

The two immobilization strategies reported in this article represent general procedures for covalent anchoring of biomacromolecules on gold surfaces, and they are, more importantly, specially adapted to the requirements of biological applications. Both pathways, first SAM I as a ready-to-use crosslinker with long-lasting reactivity, and second SAM II, which is not bioreactive until activation to its diazo derivative SAM IV, have their own applicability. SAM I provides a highly reactive surface within seconds, which is easy to pre-

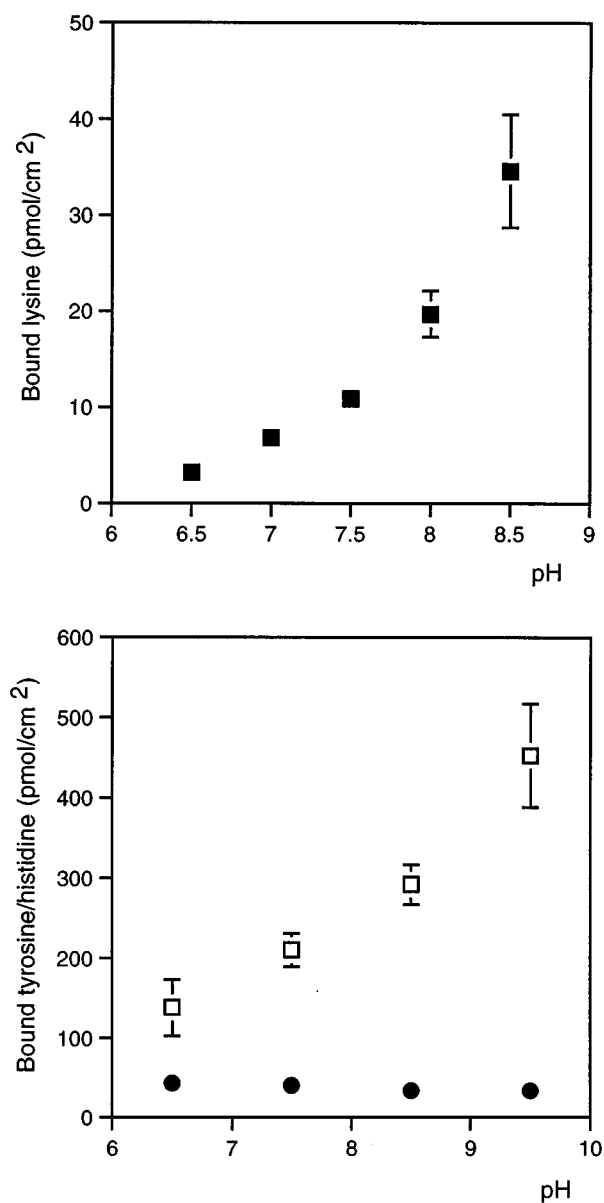


FIG. 6. pH dependence of amino acid immobilization. Top: binding of  $[^{14}\text{C}]$ -L-lysine (■) by SAM I; bottom: binding of  $[^{14}\text{C}]$ -L-tyrosine (□) and  $[^{14}\text{C}]$ -L-histidine (●) on SAM IV. The standard errors are often smaller than the symbols used.

pare and able to bind many nucleophilic groups. Hydrolysis of the activated ester groups in the monolayer arrangement (if chemisorbed on ultraflat gold) is very slow and therefore does not compete dramatically with the binding of the target. Furthermore, it has proven its applicability in several studies. In contrast, SAM II needs some further activation steps, but is then, as SAM IV, selective toward activated aromatic groups. This could be valuable for site-specific immobilization of proteins or other structures labeled with aromatic functionalities. It can be totally quenched upon warmup, compared to SAM I, which retains its reactivity for days, and is cleavable by reduction to perform reversible covalent anchoring.

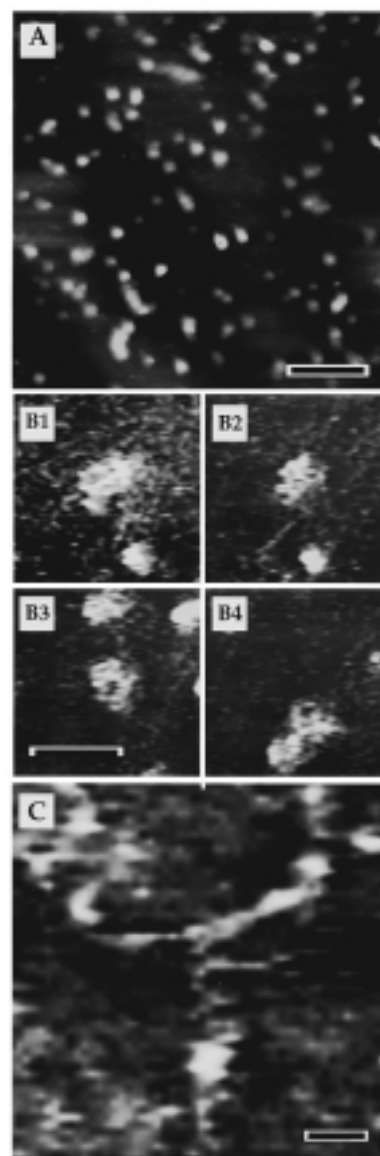


FIG. 7. Disassembly of clathrin cages to triskelia visualized by AFM *in situ* under native conditions in aqueous buffers. (A) clathrin cages before starting the disassembly, immobilized at a concentration of 1  $\mu\text{g}/\text{ml}$  in 0.1 M MES (pH 6.5), 0.5 mM  $\text{MgCl}_2$ , 1 mM EGTA, 0.02%  $\text{NaN}_3$ . The height of the cages was  $16 \pm 6$  nm; bar: 1  $\mu\text{m}$ . (B) 10 min after the exchange of the buffer with 0.5 M Tris/Cl (pH 7.0) showing basketlike intermediate structures. The height of the baskets was approximately 2 nm; bar: 500 nm. (C) Regularly spread out triskelion; bar: 20 nm.

## ACKNOWLEDGMENTS

This work was supported in part by grants of the ETH Zurich, the Swiss National Science Foundation, Ciba-Geigy Jubilaeums-Stiftung Basel, the Schweizerische Krebsliga, and the Schweizerische Reinraumgesellschaft.

- <sup>1</sup>R. G. Nuzzo and D. L. Allara, *J. Am. Chem. Soc.* **105**, 4481 (1983).
- <sup>2</sup>C. D. Bain, E. B. Troughton, Y.-T. Tao, J. Evall, G. M. Whitesides, and R. G. Nuzzo, *J. Am. Chem. Soc.* **111**, 321 (1989).
- <sup>3</sup>G. M. Whitesides and P. E. Laibinis, *Langmuir* **6**, 87 (1990).
- <sup>4</sup>R. G. Nuzzo, F. A. Fusco, and D. L. Allara, *J. Am. Chem. Soc.* **109**, 2358 (1987).

- <sup>5</sup>R. G. Nuzzo, E. M. Korenic, and L. A. Dubois, *J. Chem. Phys.* **93**, 767 (1990).
- <sup>6</sup>L. Strong and G. M. Whitesides, *Langmuir* **4**, 546 (1988).
- <sup>7</sup>C. E. D. Chidsey, G.-Y. Liu, P. Rowntree, and G. Scoles, *J. Chem. Phys.* **91**, 4421 (1989).
- <sup>8</sup>N. Camillone III, C. E. D. Chidsey, G.-Y. Liu, and G. Scoles, *J. Chem. Phys.* **98**, 3503 (1993).
- <sup>9</sup>C. E. D. Chidsey and D. N. Loiacono, *Langmuir* **6**, 682 (1990).
- <sup>10</sup>P. Fenter, P. Eisenberger, and K. S. Liang, *Phys. Rev. Lett.* **70**, 2447 (1993).
- <sup>11</sup>M. G. Samant, C. A. Brown, and J. G. Gordon, *Langmuir* **7**, 437 (1991).
- <sup>12</sup>S. D. Evans, R. Sharma, and A. Ulman, *Langmuir* **7**, 156 (1991).
- <sup>13</sup>J. P. Folkers, P. E. Laibinis, and G. M. Whitesides, *Langmuir* **8**, 1330 (1992).
- <sup>14</sup>T. Han and T. P. Beebe, *Langmuir* **10**, 2705 (1994).
- <sup>15</sup>C. A. Widrig, C. Chung, and M. D. Porter, *J. Electroanal. Chem.* **310**, 335 (1991).
- <sup>16</sup>Y. T. Kim and A. J. Bard, *Langmuir* **8**, 1096 (1992).
- <sup>17</sup>C. A. Alves, E. L. Smith, and M. D. Porter, *J. Am. Chem. Soc.* **114**, 1222 (1992).
- <sup>18</sup>E. Delamarche, B. Michel, Ch. Gerber, D. Anselmetti, H.-J. Güntherodt, H. Wolf, and H. Ringsdorf, *Langmuir* **10**, 2869 (1994).
- <sup>19</sup>D. Anselmetti, A. Baratoff, H.-J. Güntherodt, E. Delamarche, B. Michel, Ch. Gerber, H. Kang, H. Wolf, and H. Ringsdorf, *Europhys. Lett.* **27**, 365 (1994).
- <sup>20</sup>C. Schönenberger, J. A. M. Sondag-Huethorst, J. Jorritsma, and L. G. J. Fokkink, *Langmuir* **10**, 611 (1994).
- <sup>21</sup>M. Salmeron, G. Neubauer, A. Folch, M. Tomitori, F. Ogletree, and P. Sautet, *Langmuir* **9**, 3600 (1993).
- <sup>22</sup>G. E. Poirier and M. J. Tarlov, *Langmuir* **10**, 2853 (1994).
- <sup>23</sup>J. P. Bucher, L. Santesson, and K. Kern, *Langmuir* **10**, 979 (1994).
- <sup>24</sup>S. Karrasch, M. Dolder, F. Schabert, J. Ramsden, and A. Engel, *Biophys. J.* **65**, 2437 (1993).
- <sup>25</sup>A. Ulman, *An Introduction to Ultra-Thin Organic Films From Langmuir–Blodgett to Self-Assembly* (Academic, San Diego, 1991).
- <sup>26</sup>L. Häussling, B. Michel, H. Ringsdorf, and H. Rohrer, *Angew. Chem. Int. Ed. Engl.* **30**, 569 (1991).
- <sup>27</sup>M. Sprik, E. Delamarche, B. Michel, U. Röthlisberger, M. L. Klein, H. Wolf, and H. Ringsdorf, *Langmuir* **10**, 4116 (1994).
- <sup>28</sup>P. Wagner, M. Hegner, H.-J. Güntherodt, and G. Semenza, *Langmuir* **11**, 3867 (1995).
- <sup>29</sup>M. Hegner, P. Wagner, and G. Semenza, *Surf. Sci.* **291**, 39 (1993).
- <sup>30</sup>P. Wagner, P. Kernen, M. Hegner, E. Ungewickell, and G. Semenza, *FEBS Lett.* **356**, 267 (1994).
- <sup>31</sup>U. Dammer, O. Popescu, P. Wagner, D. Anselmetti, H.-J. Güntherodt, and G. N. Misevic, *Science* **267**, 1173 (1995).
- <sup>32</sup>P. Wagner, M. Hegner, P. Kernen, F. Zaugg, and G. Semenza, *Biophys. J.* (in press).
- <sup>33</sup>R. L. McCarley, D. J. Dunaway, and R. J. Willicut, *Langmuir* **9**, 2775 (1993).
- <sup>34</sup>J. A. M. Sondag-Huethorst, C. Schönenberger, and L. G. J. Fokkink, *J. Phys. Chem.* **98**, 6826 (1994).